FLUID FLOW AND HEAT TRANSFER IN CALENDERING

J. VLACHOPOULOS

and

E. MITSOULIS

Department of Chemical Engineering
McMaster University
Hamilton, Ontario
Canada L8S4L7

I. INTRODUCTION

1. The Calendering Process

The term "calender" is derived from the Greek *Kylindros* (cylinder) and according to Webster's International Dictionary, it means "to press (as cloth, rubber, paper) between rollers or plates in order to make smooth and glossy or glazed or to thin into sheets". The calendering of molten polymers is a process for the production of continuous sheet or film by squeezing the melt between a pair of heated counter-rotating rolls.

The modern technological developments in the calendering of thermoplastic materials are offshoots of the art of fabric and rubber calendering, which dates back to the early 1800's. Elden and Swan[1] present a short history and a detailed account of the major technological developments up to about 1968.

Industrial calenders consist usually of 3-6 rotating rolls in a *Z* or *L* arrangement. The basic forming operation is completed by the calender itself and is normally followed by additional treatment of the plastic sheet or film produced. A typical calendering layout is shown in Fig. 1

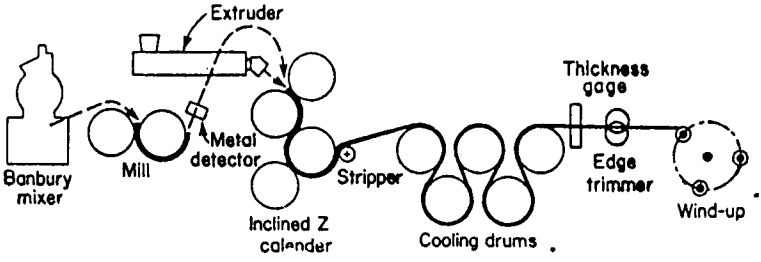

Figure 1. A typical calendering layout.

(from Marshall[2]). The molten material is fed to the calender rolls from a Banbury mixer and two-roll mill system or from a large extruder. Calender sizes range up to 90 cm in diameter and 250 cm wide, with polymer throughputs up to 4000 kg/hr, according to Tadmor and Gogos[3]. Roll speeds may be as high as 2 m/s for certain thin flexible films (thickness less than 0.1 mm). Calendering lines are very expensive in terms of capital investment in machinery. Film and sheet extrusion are competitive processes because the capital investment for the extruder itself is only a fraction of the cost of a calender. However, the high quality and volume capabilities of calendering lines make them advantageous for many types of products, especially for temperature sensitive materials. Polyvinyl chloride (PVC) is the major polymer that is calendered.

2. Literature Survey

a. Mathematical Modeling The quality of the sheet or film produced is determined by the flow and heat transfer phenomena in the gap between two rotating rolls. It is thus of great importance to determine the velocity and temperature profiles as the melt is squeezed between the rolls (see Fig. 2), the pressure distribution on the roll surfaces, the roll separating force and the torque and energy input. One of the earliest attempts to model this process was published by Ardichvili[4]. Eley[5,6] presented a somewhat different analysis and Finston[7] included thermal effects. It is, however, a rather realistic Newtonian flow analysis by Gaskell[8] that spearheaded further developments in modeling. An attempt to include viscoelastic effects was presented by Paslay[9]. The major conclusions of these early investigations were summarized by Marshall[3].

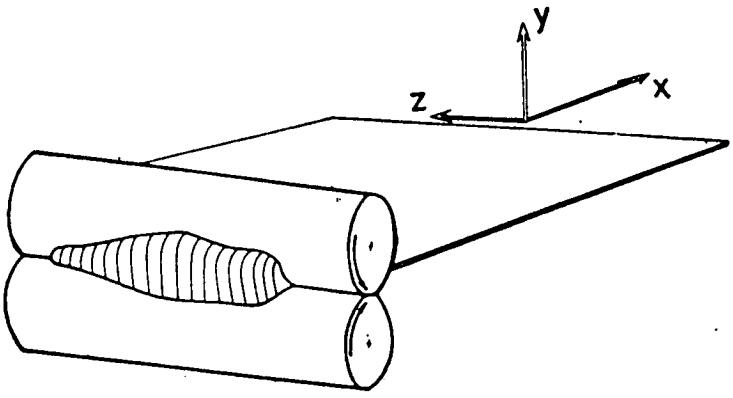

Figure 2. Schematic representation of molten polymer sheet passing through a calender.

Mc Kelvey[10] reworked Gaskell's model for Newtonian flow and extended it to inclnde non-Newtonian (i.e. shear-thinning) effects. Brazinsky et al[11] presented an analysis for power-law fluids and Alston and Astill[12] for a hyperbolic tangent viscosity model. Some inaccuracies in McKelvey's[10] power consumption calculations were corrected by Ehrmann and Vlachopoulos[13]. The asymmetrical problem was treated analytically using bipolar cylindrical coordinates by Ehrlich and Slattery[14] and by Takserman-Krozer et al[15]. Renert[16] provided an approximate solution for the pressure profile in the nip for the power-law model. Reher and Grader[17] presented a numerical solution for the non-Newtonian problem. Some experimental results and numerical calculations on temperature development due to viscous dissipation were reported by Torner[18]. Viscoelasticity was taken into account in the investigations of Tokita and White[19], Chong[20] and White[21].

Kiparissides and Vlachopoulos[23] developed a finite element analysis for symmetric and asymmetric calendering (different roll speeds, different roll diameters). Viscous dissipation effects were included in finite difference solutions of the energy equation in bipolar coordinates by Bekin et al[28] and by Kiparissides and Vlachopoulos[24] in rectangular coordinates. The non-isothermal problem was also treated by the method of orthogonal collocation by Dobbels and Mewis[25]. Agassant and co-workers[26,27,28] presented a method for the calculation of the average temperature rise and several calculations of separating forces, torques and the critical conditions for the appearance of defects in calendered sheets. Nonisothermal calculations were also carried out by Dimitrijew and Sporjagin[29] by the finite difference method and by Woskressenski et al[30] by the finite element method. Seeger et al[31] presented a finite element solution and calculated velocity and stress profiles for a power-law fluid.

An isothermal model with slip was developed by Vlachopoulos and Hrymak[32] using the lubrication approximation and a Runge-Kutta solution. Other investigations were carried out by Chung for Binghan plastic fluids[33] and compressible fluids[34], by Suto and co-workers[35-37] for Newtonian and viscoelastic fluids and by Lee et al[38] for a Maxwell fluid.

b. Experimental Investigations There have been very few experimental investigations that were published in the open literature. For a long time, Bergen and Scott's[39] measurements on a plasticized resin were the only basis for comparison of the proposed mathematical models. Direct comparisons could not be made, however, because of limited information on the rheological properties of the resin. Unkrüer[40] carried out a detailed experimental study of calendering of Polyvinyl Chloride (PVC) and Poly-

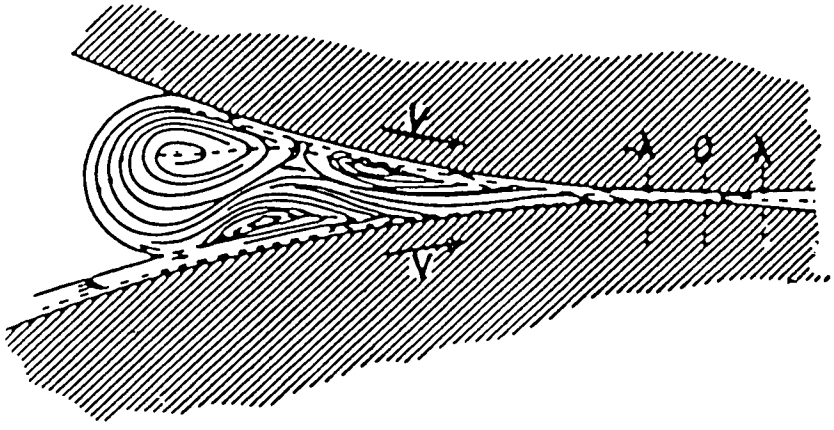

Figure 3. (a) Flow pattern in the melt bank

styrene (PS). Using color tracers he observed a complex flow pattern with three recirculation regions in the melt bank and flow in the axial (cross-machine) direction as shown in Fig. 3. In Unkrüer's thesis[40] there is limited

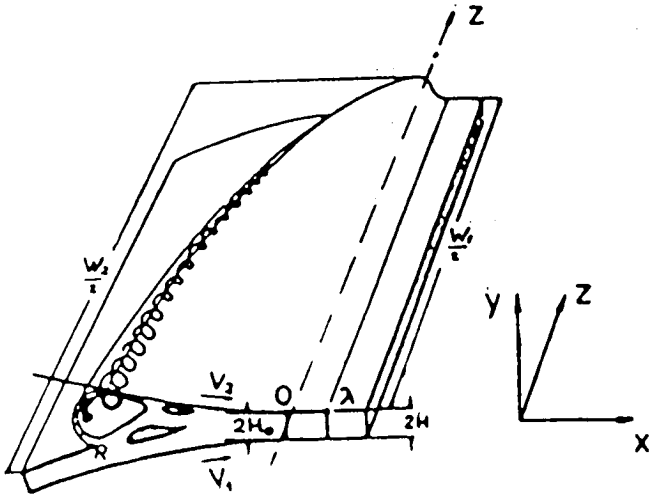

Figure 3. (b) Flow in the axial (cross-machine) direction

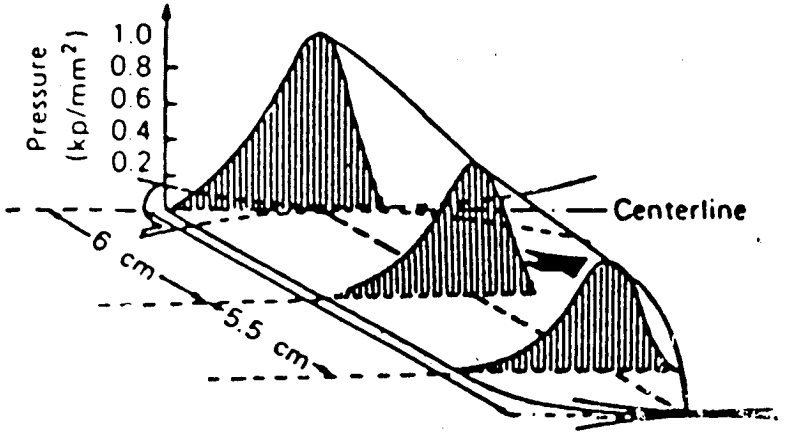

Figure 3. (c) Pressure profiles at different axial positions. (According to Unkrüer[40])

amount of rheological data of the melts and thus a direct comparison of model predictions and experimental measurements on pressure distribution is impossible.

Agassant[36] carried out an extensive experimental study on calendering (using PVC and a silicone oil for certain measurements) and compared his results to model predictions for separating forces and torques. Visualization studies of the complex flow pattern (similar to Unkrüer's[40]) in the melt bank were also included in Agassant's work as well as studies on the origin and appearance of calendered sheet defects. An investigation on the surface irregularity Polypropylene (PP) sheet was carried out by Prentice[41]. Limited amount of experimental data was also given by Hatzmann et al[42], Kopsch[43] and Suto[35-37].

Vlachopoulos and Hrymak[33] presented pressure distribution and torque measurements for rigid PVC carried out by Chauffoureaux[44], as well as measurements of apparent viscosity and slip velocity for a wide range of temperatures.

II. LUBRICATION APPROXIMATION

1. General Considerations

Polymer melts flow at low Reynolds numbers, e.g. $Re = 10^{-2} - 10^{-4}$, and the creeping flow approximation is applicable[45]. Thus, the conservation equations for steady flow are

$$\nabla\cdot(\rho v) = 0 \tag{1}$$

$$0 = -\nabla p + \nabla\cdot\tau \tag{2}$$

$$\rho C_p v\cdot\nabla T = \nabla\cdot(k\nabla T) + p\nabla\cdot v + \tau:\Delta v \tag{3}$$

where ρ represents density, v velocity vector, p pressure, τ extra stress tensor, C_p specific heat, T temperature and k thermal conductivity.

Polymer melt compressibility may be important in certain processes (see Tadmor and Gogos[3]), but not in calendering. Chung's results[34] are for uncharacteristically high calendering pressures. C_p and k can be assumed constant. Thus the above equations reduce to

$$\nabla\cdot v = 0 \tag{4}$$

$$0 = -\nabla p + \nabla\cdot\tau \tag{5}$$

$$\rho C_p v\cdot\nabla T = k\nabla^2 T + \tau:\nabla v \tag{6}$$

Further assuming that the fluid does not spread as it enters the gap between the rolls, we may write equations (4), (5) and (6) for two dimensions, where x is the direction of flow and y perpendicular to roll axis, as

$$\frac{\partial v_x}{\partial x} + \frac{\partial v_y}{\partial y} = 0 \tag{7}$$

$$0 = -\frac{\partial p}{\partial x} + \frac{\partial \tau_{xx}}{\partial x} + \frac{\partial \tau_{xy}}{\partial y} \tag{8}$$

$$0 = -\frac{\partial p}{\partial y} + \frac{\partial \tau_{yx}}{\partial x} + \frac{\partial \tau_{yy}}{\partial y} \tag{9}$$

$$\rho C_p \left(v_x \frac{\partial T}{\partial x} + v_y \frac{\partial T}{\partial y} \right) = k \left(\frac{\partial^2 T}{\partial x^2} + \frac{\partial^2 T}{\partial y^2} \right) + \tau_{xx} \frac{\partial v_x}{\partial x} + \tau_{xy} \frac{\partial v_x}{\partial y} + \tau_{yx} \frac{\partial v_y}{\partial x} + \tau_{yy} \frac{\partial v_y}{\partial y} \tag{10}$$

It is also reasonable to assume that the flow in the gap will be nearly parallel so that $\partial/\partial x \ll \partial/\partial y$, $v_y \ll v_x$, $v_x = v_x(x, y)$ and $p = p(x)$, thus we have

$$\frac{\partial v_x}{\partial x} + \frac{\partial v_y}{\partial y} = 0 \tag{11}$$

$$0 = -\frac{\partial p}{\partial x} + \frac{\partial}{\partial y}(\tau_{xy}) \tag{12}$$

$$\rho C_p v_x \frac{\partial T}{\partial x} = k \frac{\partial^2 T}{\partial y^2} + \tau_{xy} \frac{\partial v_x}{\partial y} \tag{13}$$

Problems that can be described by equations (11) and (12) are said to obey the *lubrication approximiation*[3,45-47]. The continuity equation (11) may be replaced by the integral form

$$Q = 2 \int_0^{h(x)} v_x \, dy \tag{14}$$

where Q is the volume rate of flow. To solve the above equations we also need a constitutive equation that relates stress to the rate of strain.

2. The Newtonian Model

For a Newtonian fluid we have

$$\tau_{xy} = \mu \frac{dv_x}{dy} \tag{15}$$

Thus the lubrication approximation equations for the rectangular coordinate system of Fig. 4 are

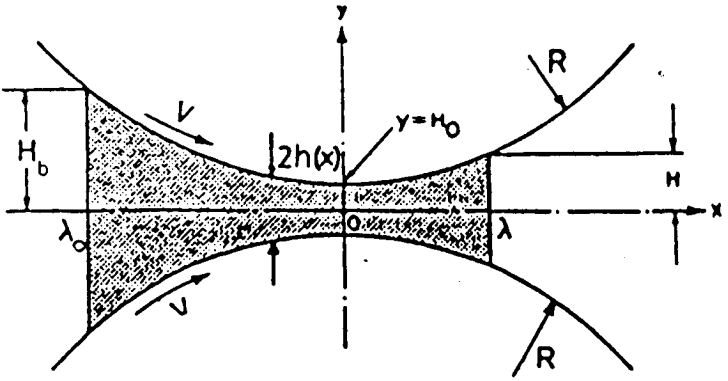

Figure 4. Notation for the lubrication flow analysis in the gap between two rotating rolls

$$Q = 2\int_0^{h(x)} v_x \, dy \tag{16}$$

$$\frac{\partial p}{\partial x} = \mu \frac{\partial^2 v_x}{\partial y^2} \tag{17}$$

Equation (17) can be solved with the no-slip and symmetry boundary conditions

$$v_x = V \text{ at } y = h(x) \tag{18}$$

$$\frac{\partial v_x}{\partial y} = 0 \text{ at } y = 0$$

to give

$$v_x = V + \frac{y^2 - h^2(x)}{2\mu} \frac{dp}{dx} \tag{19}$$

and by using the conservation of mass equation (16) we get

$$Q = 2\int_0^{h(x)} v_x \, dy = 2h(x)\left[V - \frac{h^2(x)}{3\mu} \frac{dp}{dx}\right] \tag{20}$$

or

$$\frac{dp}{dx} = \frac{3\mu}{h^2(x)}\left(V - \frac{Q}{2h(x)}\right) \tag{21}$$

The distance between roll and the centerline can be expressed with a remarkable degree of accuracy, even for relatively large distances from the minimum gap width, by the second order polynomial

$$h(x) = H_0\left(1 + \frac{x^2}{2RH_0}\right) \tag{22}$$

Introducing a dimensionless variable

$$x^* = \frac{x}{\sqrt{2RH_0}} \tag{23}$$

we have

$$\frac{h(x)}{H_0} = 1 + x^{*2} \tag{24}$$

If we assume that the sheet leaves the rolls with a thickness H and a speed V we have

$$Q = 2VH \tag{25}$$

and

$$\frac{H}{H_0} = \frac{Q}{2VH_0} \tag{26}$$

Letting $x^* = \lambda$ for $h(x) = H$ we have

$$\frac{H}{H_0} = \frac{Q}{2VH_0} = 1 + \lambda^2 \tag{27}$$

Substituting Q with $(1 + \lambda^2)\, 2VH_0$ and rearranging equation (21), we get

$$\frac{dp^*}{dx^*} = \sqrt{\frac{18\,R}{H_0}}\,\frac{x^{*2} - \lambda^2}{(1 + x^{*2})^3} \tag{28}$$

where

$$p^* = \frac{pH_0}{\mu V} \tag{29}$$

Equation (28) gives zero pressure gradient at $x^* = \pm\lambda$. The distance $x^* = \lambda$ represents the point where the sheet leaves the rolls and $x^* = -\lambda$ is the point of maximum pressure. Upon integration, with $p^*(\lambda) = 0$, equation (28) becomes

$$p^* = \sqrt{\frac{9R}{32\,H_0}}\left[\frac{x^{*2}(1 - 3\lambda^2) - 1 - 5\lambda^2}{(1 + x^{*2})^2}\,x^* + (1 - 3\lambda^2)(\tan^{-1}x^* - \tan^{-1}\lambda) + \frac{1 + 3\lambda^2}{1 + \lambda^2}\lambda\right] \tag{30}$$

The pressure distribution has a maximum at $x^* = \lambda$ given by

$$p^*_{max} = \frac{3C(\lambda)}{2}\sqrt{\frac{R}{2H_0}} \tag{31}$$

where

$$C(\lambda) = \frac{1 + 3\lambda^2}{1 + \lambda^2}\,\lambda - (1 - 3\lambda^2)\tan^{-1}\lambda \tag{32}$$

and becomes zero at $x^* = \lambda$ where the polymer leaves the rolls and at $x^* = -\lambda_0$ where the rolls "bite" on the polymer. The relation between $-\lambda_0$ and λ is unique. McKelvey's[10] results are slightly in error. Such errors cause large deviations in power consumption calculations[12]. Fig. 5 gives the λ_0 versus λ relationship based on calculations by Ehrmann and Vlachopoulos[13]. Pressure distributions are shown in Fig. 6 for different leave-off distances λ.

If we assume that $p \to 0$ as $x^* \to -\infty$ we get

$$\lambda_\infty = 0.475 \tag{33}$$

For that value of λ we have the maximum sheet thickness to minimum gap width ratio

$$\frac{H_{max}}{H_0} = 1 + \lambda_\infty^2 = 1.226 \tag{34}$$

The velocity can be easily obtained from equation (19) with the help of equation (28) and can be expressed as

$$v_x^* = 1 + \frac{3}{2}\frac{(1 - y^{*2})(\lambda^2 - x^{*2})}{(1 + x^{*2})} \tag{35}$$

where

$$v_x^* = \frac{v_x}{V} \quad \text{and} \quad y^* = \frac{y}{H_0} \tag{36}$$

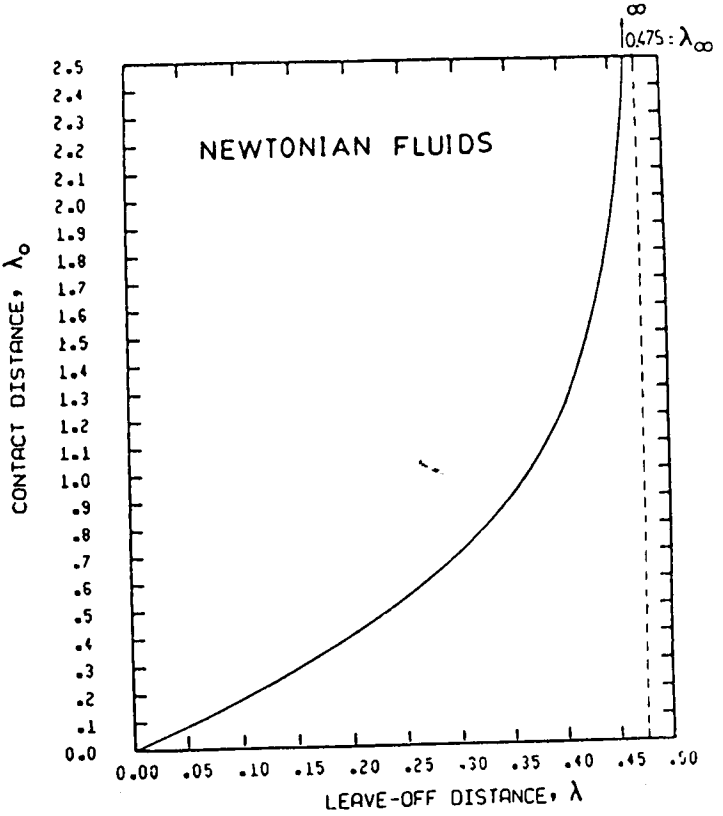

Figure 5. Relationship between λ_0, the distance from minimum gap width where the rolls "bite" on the polymer, and λ the leave-off distance (Newtonian model).

A schematic diagram of the velocity profiles is shown in Fig. 7. We note that the velocity at the centerline becomes zero (stagnation point) when

$$x^* = -\sqrt{2 + 3\lambda^2} \tag{37}$$

For $\lambda = 0.425$ the stagnation point occurs at the entry $-\lambda_0$. Thus for $\lambda > 0.425$ a recirculatory flow pattern develops in the entrance region as shown schematically in Fig. 7.

From the above results it is easy to calculate the separating forces, torques and the power consumed (see for example Tadmor and Gogos[3], McKelvey[10] and Middleman[47]).

3. The Power-Law Model

For a power-law fluid with

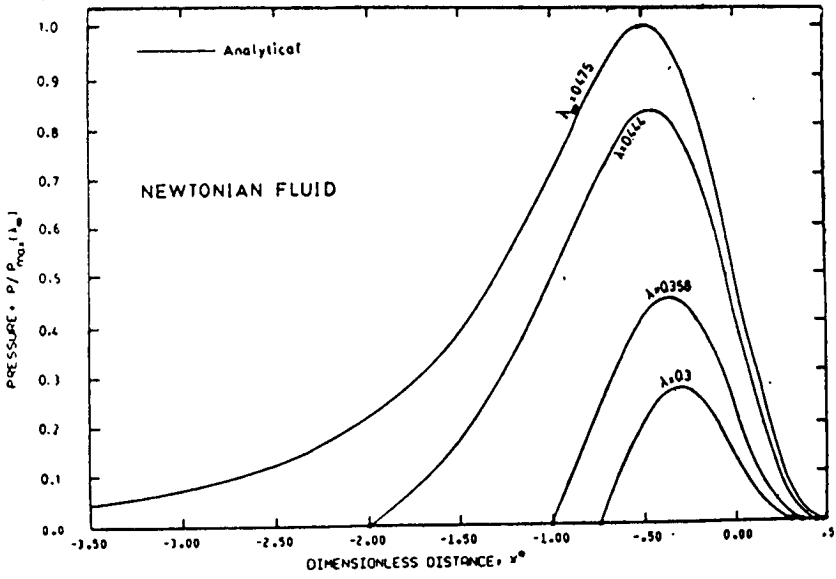

Figure 6. Pressure distributions for different leave-off distances (Newtonian model).

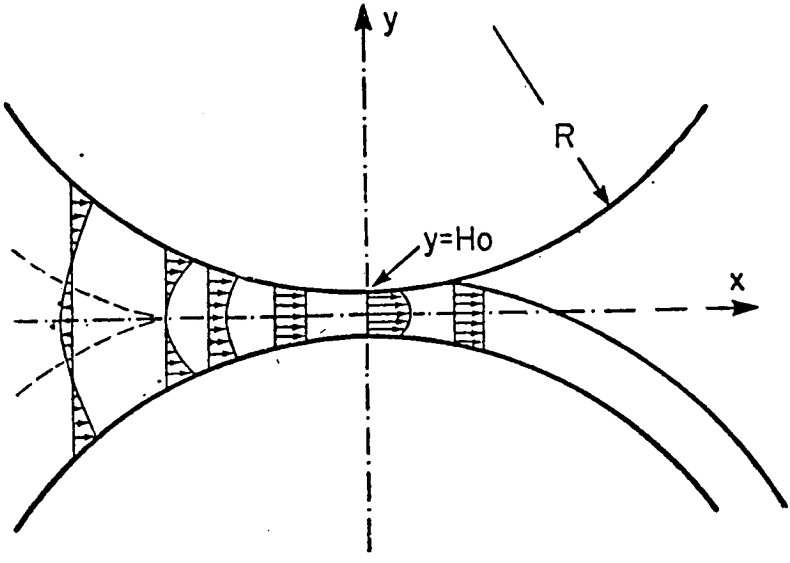

Figure 7. Schematic diagram of velocity profiles.

$$\tau_{xy} = m\left(\frac{\partial v_x}{\partial y}\right)^n \tag{38}$$

the lubrication approximation equations are

$$Q = 2\int_0^{h(x)} v_x\, dy \tag{39}$$

$$\frac{\partial p}{\partial x} = m\frac{\partial}{\partial y}\left(\frac{\partial v_x}{\partial y}\right)^n \tag{40}$$

From the Newtonian model we anticipate two flow regions, a region where the pressure gradient is positive ($-\lambda < x^* < \lambda$) and a region where the pressure gradient is negative ($-\lambda_0 < x^* < -\lambda$). Thus we should integrate equation (40) separately for each region. We have

$$v_x = V + \frac{n}{n+1}\left(\frac{1}{m}\frac{dp}{dx}\right)^{1/n}(y^{n+1/n} - h(x)^{n+1/n}) \tag{41}$$

$$v_x = V - \frac{n}{n+1}\left(-\frac{1}{m}\frac{dp}{dx}\right)^{1/n}(y^{n+1/n} - h(x)^{n+1/n}) \tag{42}$$

Introducing either one of the above equations into the integral of equation (39) and then solving for the pressure gradient, we get

$$\frac{dp^*}{dx^*} = -\left(\frac{2n+1}{n}\right)^n\left(\frac{2R}{H_0}\right)^{1/2}\frac{(\lambda^2 - x^{*2})\,|\,\lambda^2 - x^{*2}\,|^{n-1}}{(1+x^{*2})^{2n+1}} \tag{43}$$

where

$$p^* = \frac{p}{m}\left(\frac{H_0}{V}\right)^n \tag{44}$$

This equation is valid for both flow regions i.e. for $-\infty < x^* < -\lambda$ where the pressure gradient is positive and for $-\lambda < x^* < \lambda$ where the pressure gradient is negative. Integrating equation (43) from x^* to λ we get

$$p^* = \left(\frac{2n+1}{n}\right)^n\left(\frac{2R}{H_0}\right)^{1/2}\int_{x^*}^{\lambda}\frac{|\,\lambda^2 - x^{*2}\,|^{n-1}\,(\lambda^2 - x^{*2})}{(1+x^{*2})^{2n+1}}\,dx^* \tag{45}$$

At $x^* = -\lambda$ the pressure dissribution has a maximum, so we may write

$$p^*_{\max} = \left(\frac{2n+1}{n}\right)^n\left(\frac{2R}{H_0}\right)^{1/2}\int_{-\lambda}^{\lambda}\frac{(\lambda^2 - x^{*2})^n}{(1+x^{*2})^{2n+1}}\,dx^* \tag{46}$$

When the calender is fed with a thermoplastic melt from an infinite reservoir we may assume that p^* vanishes as $x^* \to -\infty$. Consequently, the value of parameter λ may be determined from

$$0 = \int_{-\infty}^{\lambda}\frac{|\,\lambda^2 - x^{*2}\,|^{n-1}(\lambda^2 - x^{*2})}{(1+x^{*2})^{2n+1}}\,dx^* \tag{47}$$

The corresponding value of the sheet thickness at the point of separation from the rolls can be calculated from equation (24), i.e.

$$\frac{H}{H_0} = 1 + \lambda^2 \tag{48}$$

The dependence of λ_∞ and H_{max} on the power-law index n is shown in Fig. 8 (see also Middleman[47] and Vlachopoulos and Hrymak[82]).

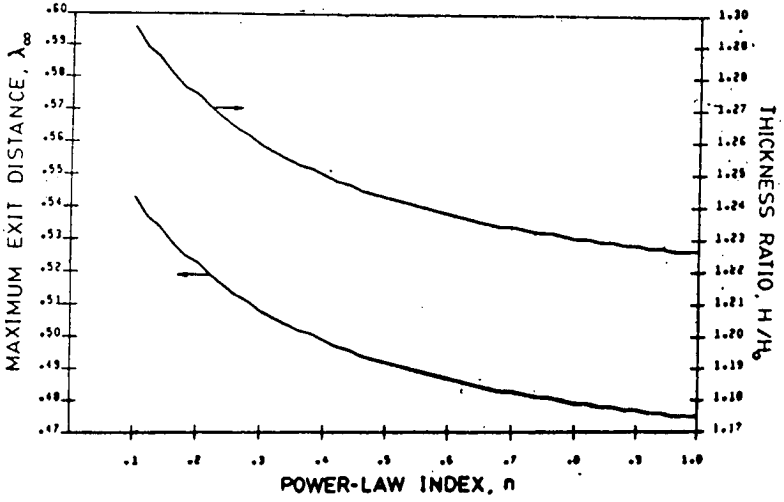

Figure 8. Leave-off distance λ and sheet thickness as a function of power-law index n for infinite feed.

4. The Power-Law Model with Slip

Vlachopoulos and Hrymak[82] developed a lubrication approximation analysis with slip. Based on measurements by Chaffoureaux et al[48] the slip velocity was assumed to obey the relation

$$V_s = V_0 + \frac{1}{\beta}\tau_w^\alpha \tag{49}$$

where τ_w is the shear stress at the wall and V_0, β and α experimentally determined constants.

The analysis begins with the simplified momentum equation

$$\frac{\partial p}{\partial x} = \frac{\partial}{\partial y}(\tau_{xy}) \tag{50}$$

where

$$\tau_{xy} = m\left(\frac{\partial v_x}{\partial y}\right)^n \tag{51}$$

The boundary conditions for calendering with slip at the roll surface are

$$\text{at } y = 0 \qquad \frac{\partial v_x}{\partial y} = 0 \tag{52}$$

$$\text{at } y = h(x) \qquad v_x = V - V_0 - \frac{1}{\beta}\tau_w^\alpha$$

Upon integrating the momentum equation and after applying the boundary conditions an expression for the velocity profile in the region where the pressure gradient is positive was obtained

$$v_x = \frac{n}{n+1}\left(\frac{1}{m}\frac{\partial p}{\partial x}\right)^{1/n}(y^{(n+1)/n} - h(x)^{(n+1)/n}) + V - V_0 - \frac{1}{\beta}\left(\frac{\partial p}{\partial x}\right)^{\alpha} h(x)^{\alpha} \quad (53)$$

and another expression for the region of negative pressure gradient

$$v_x = -\frac{n}{n+1}\left(-\frac{1}{m}\frac{\partial p}{\partial x}\right)^{1/n}(y^{(n+1)/n} - h(x)^{(n+1)/n}) + V - V_0 - \frac{1}{\beta}\left(-\frac{\partial p}{\partial x}\right)^{\alpha} h(x)^{\alpha} \quad (54)$$

Either of equations for the velocity profile may then be integrated to give the volumetric flow rate

$$Q = 2\int_0^{h(x)} v_x \, dy \quad (55)$$

The result may be written as

$$\frac{Q}{2h} = V - V_0 - \frac{1}{\beta}\left(\frac{\partial p}{\partial x}\right)^{\alpha} h(x)^{\alpha} - \frac{n}{(2n+1)}\left(\frac{1}{m}\frac{\partial p}{\partial x}\right)^{1/n} h(x)^{(n+1)/n} \quad (56)$$

It turns out that it is convenient to introduce certain dimensionless variables

$$x^* = \frac{x}{\sqrt{2RH_0}} \quad (57)$$

$$\lambda^2 = \frac{Q}{2(V - V_0)H_0} - 1 \quad (58)$$

and from geometrical considerations (equation (24))

$$h(x) = H_0(1 + x^{*2}) \quad (59)$$

After transforming both sides of Equation (56) and rearranging we obtain

$$\left(\frac{\partial p}{\partial x^*}\right)\left\{B\left|\frac{\partial p}{\partial x^*}\right|^{\alpha-1} + C\left|\frac{\partial p}{\partial x^*}\right|^{1-n/n}\right\} - A = 0 \quad (60)$$

where

$$A = \frac{(V - V_0)}{(1 + x^{*2})}(x^{*2} - \lambda^2)$$

$$B = \frac{1}{\beta} H_0^{\alpha}(1 + x^{*2})^{\alpha}(2RH_0)^{-\alpha/2} \quad (61)$$

$$C = \frac{n}{(2n+1)}\left(\frac{1}{m}\right)^{1/n}(2RH_0)^{-1/2n} H_0^{(n+1)/n}(1 + x^{*2})^{(n+1)/n}$$

Equation (60) was solved numerically by using a modified linear interpolation technique[49] to give the pressure gradient $(\partial p/\partial x^*)$ for a large number of x^* positions. The pressure distribution was then calculated by introducing the pressure gradient values into a fourth-order Runge-Kutta formula[32,49], starting from $x^* = \lambda$ and $p = 0$.

Comparisons between the lubrication approximation theory and experimental measurements[32] are shown in Fig. 9. While the lubrication theory with slip predicts a pressure distribution closer to the experimental data than the theory without slip, there is still considerable deviation. The

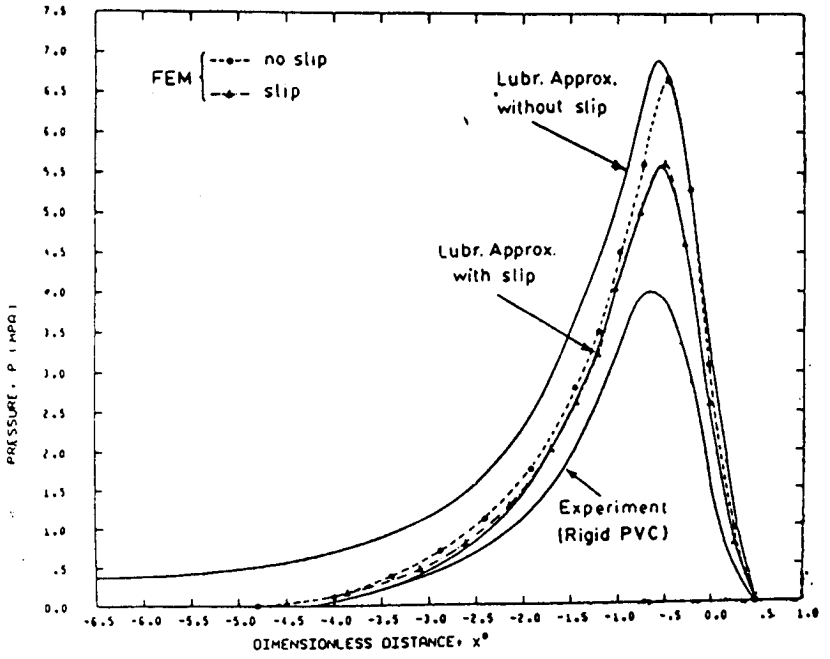

Figure 9. Comparison between predicted and measured pressure distributions for the data given by Vlachopoulos and Hrymak[32].

torques measured on the rolls were 353J and 226J while the calculated values using the lubrication model with slip were 253J and 213J, respectively. The deviations were believed to be due to uncertainties in temperature in this isothermal flow analysis[32].

5. Non-Isothermal Flow

Finston[7] seems to have made the first attempt to treat the non-isothermal problem. It is, however, Petrusanskii's work[50] as reported by Torner[18] and the subsequent analysis by Kiparissides and Vlachopoulos[34] that gave a detailed information on the development of a temperature profile due to viscous dissipation.

The non-isothermal analysis starts with the simplified equations

$$Q = 2\int_0^{h(x)} v_x \, dy \tag{62}$$

$$\frac{\partial p}{\partial x} = \frac{\partial}{\partial y}(\tau_{xy}) \tag{63}$$

$$\rho C_p v_x \frac{\partial T}{\partial x} = k \frac{\partial^2 T}{\partial y^2} + \tau_{xy}\left(\frac{\partial v_x}{\partial y}\right) \tag{64}$$

where

$$\tau_{xy} = m\left(\frac{\partial v_x}{\partial y}\right)^n \text{ and } m = m(T) \tag{65}$$

Finite difference solution[18,24] of the above equations yields a rather peculiar development of a temperature profile due to viscous dissipation as shown in Fig. 10. These analyses suggest that a temperature rise of several degrees

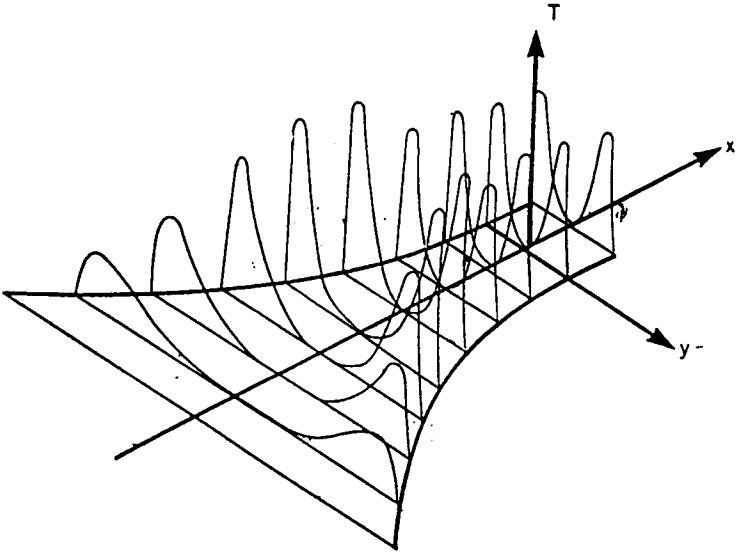

Figure 10. Schematic representation of temperature development due to viscous dissipation

is possible because of viscous dissipation and may have detrimental effects for temperature sensitive materials.

III. TWO-DIMENSIONAL ANALYSIS

The need for a fully two-dimensionnal model of calendering became apparent because of the inability of the lubrication approximation to describe the flow for large entrance angles and to account for recirculation phenomena in the melt bank. Mitsoulis et al[51–54] used their MACVIP finite element program[55] to solve the two-dimensional creeping flow equations:

$$\frac{\partial v_x}{\partial x} + \frac{\partial v_y}{\partial y} = 0 \tag{66}$$

$$0 = -\frac{\partial p}{\partial x} + \frac{\partial \tau_{xx}}{\partial x} + \frac{\partial \tau_{yx}}{\partial y} \tag{67}$$

$$0 = -\frac{\partial p}{\partial y} + \frac{\partial \tau_{xy}}{\partial x} + \frac{\partial \tau_{yy}}{\partial y} \tag{68}$$

$$\rho C_p \left(v_x \frac{\partial T}{\partial x} + v_y \frac{\partial T}{\partial y} \right) = k \left(\frac{\partial^2 T}{\partial x^2} + \frac{\partial^2 T}{\partial y^2} \right) + \tau_{xx} \frac{\partial v_x}{\partial x} + \tau_{yx} \frac{\partial v_x}{\partial y} + \tau_{yx} \frac{\partial v_y}{\partial x} + \tau_{yy} \frac{\partial v_y}{\partial y} \tag{69}$$

where, for a generalized Newtonian fluid (power-law model), we have

$$\tau_{xx} = 2\eta(\dot{Y}) \frac{\partial v_x}{\partial x} \tag{70}$$

$$\tau_{yy} = 2\eta(\dot{Y}) \frac{\partial v_y}{\partial y} \tag{71}$$

$$\tau_{yx} = \tau_{xy} = \eta(\dot{Y}) \left(\frac{\partial v_y}{\partial x} + \frac{\partial v_x}{\partial y} \right) \tag{72}$$

and

$$\eta(\dot{Y}) = m \left(\frac{1}{2} I_2 \right)^{(n-1)/2} = m \left[\frac{1}{2} (\dot{Y}_{xx}^2 + (\dot{Y}_{y.}^2 + 2 \dot{Y}_{xy} \right]^{(n-1)/2} \tag{73}$$

The apparent viscosity $\eta(\dot{Y})$ will normally be a function of temperature and may also depend on pressure[3]. Under usual calendering conditions, however, pressnre dependence of viscosity will be insignificant.

Numerical calculations were carried out[52,53] for the calendering of rigid PVC data appearing in the paper of Vlachopoulos and Hrymak[33]. The pressure distributions were shown in Fig. 9 for isothermal conditions. The predictions are similar to those of the lubrication approximation. The deviations between theory and experiments are still present.

Non-isothermal calculations were carried out for Newtonian and power-law fluids for the same data as those of Kiparissides and Vlachopoulos[34]. Considerable differences were noted because in the present solution the convection term $v_y \partial T/\partial y$ as well as the rest of the terms that were omitted in the lubrication analysis give rise to higher temperatures at the centerline and higher maxima as shown in Fig. 11. A three-dimensional plot of temperature development due to viscous dissipation is shown in Fig. 12. When the fully non-isothermal model was applied for the data of Fig. 9 with slip, the deviation between theory and experiment became even larger. The maximum pressure was $p_{max} = 6.7$ MPa versus $p_{max} = 5.6$ MPa for assumed isothermal calendering at 182°C and $p_{max} = 4.0$ MPa as measured.

Mitsoulis et al[53,54] also developed a method for the determination of the

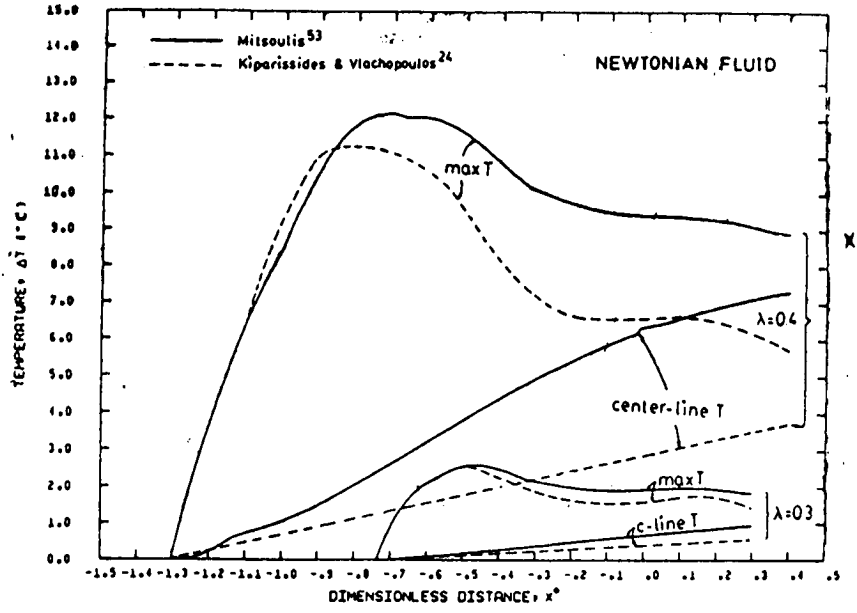

Fig. 11 Comparison between calculated temperature distributions using two-dimensional[68] and lubrication approximation[24] analyses.

free surface in the melt bank. In this method the calculations start from an assumed free surface shape. This is iteratively improved by constructing successively new surfaces which must have the properties of a streamline i.e. no cross-flow. The streamline pattern for rigid PVC calendering with slip is shown in Fig. 13 and has a striking similarity with some of Agassant's[28] experimental results. Unkrüer[40] and Agassant[28] noted also the existence of a third small vortex (see also Tadmor and Gogos[3]) but such a vortex did not appear in any of Mitsoulis et al[53,54] simulations. The predicted temperature contours are shown in Fig. 14.

IV. VISCOELASTIC EFFECTS

As mentioned in the literature survey, few attempts were made to account for the effect of viscoelasticity. While the importance of a Deborah number has been cited the results are rather inconclusive.

Mitsoulis[54] carried out some finite element calculations using the Criminale-Ericksen-Filbey constitutive equation[69] which has the general tensorial form

$$\tau = \eta\,\dot{Y} + \left(\frac{1}{2}\Psi_1 + \Psi_2\right)\{\dot{Y}\cdot\dot{Y}\} - \frac{1}{2}\Psi_1\frac{\mathcal{D}}{\mathcal{D}t}\dot{Y} \qquad (74)$$

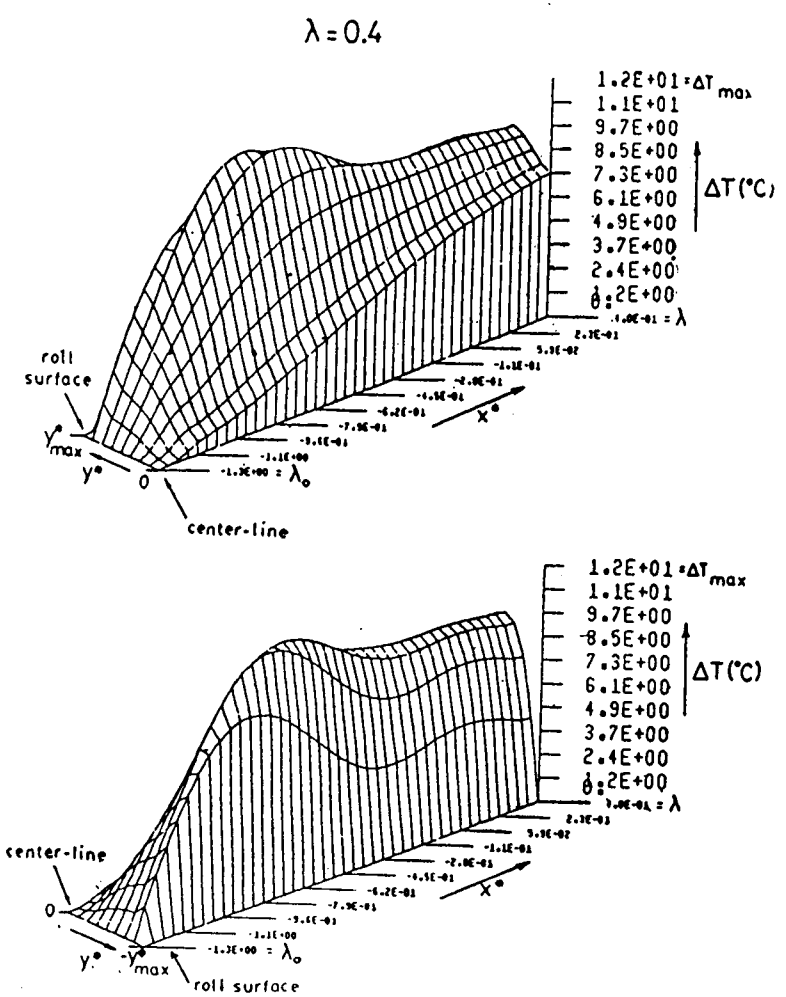

Fig. 12 Temperature development due to viscous dissipation in calendering of a Newtonian fluid.

where η, Ψ_1 and Ψ_2 are the viscosity, the first and second normal stress coefficients, respectively. These are functions of the magnitude of the rate of strain tensor

$$| \dot{Y} | = \left[\frac{1}{2} I_2\right]^{1/2} = \left[\frac{1}{2}\{\dot{Y} \cdot \dot{Y}\}\right]^{1/2} \tag{75}$$

The operator $\mathcal{D}/\mathcal{D}t$ gives the corotational or Jaumann derivative

$$\frac{\mathcal{D}}{\mathcal{D}} \dot{Y} = \frac{\mathcal{D}}{\mathcal{D}} \dot{Y}_{ij} = \frac{\partial \dot{Y}_{ij}}{\partial t} + v_k \frac{\partial}{\partial x_k} \dot{Y}_{ik} + \frac{1}{2}\{\omega_{ik} \dot{Y}_{kj} - \dot{Y}_{ik} \omega_{kj}\} \tag{76}$$

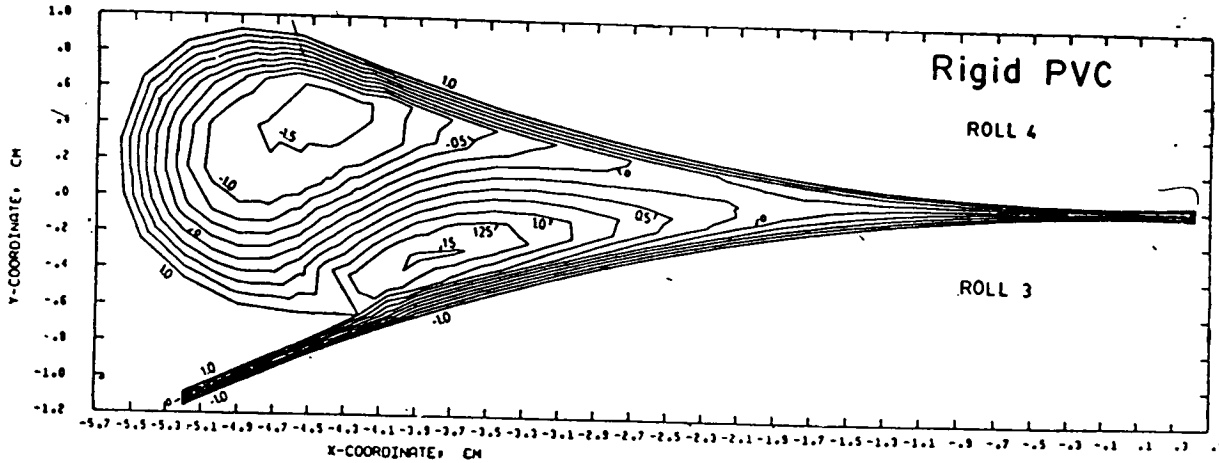

Fig. 13 Streamline pattern for calendering of rigind PVC with slip (for the calendering conditions and property data of Vlachopoulos and Hrymark[32])

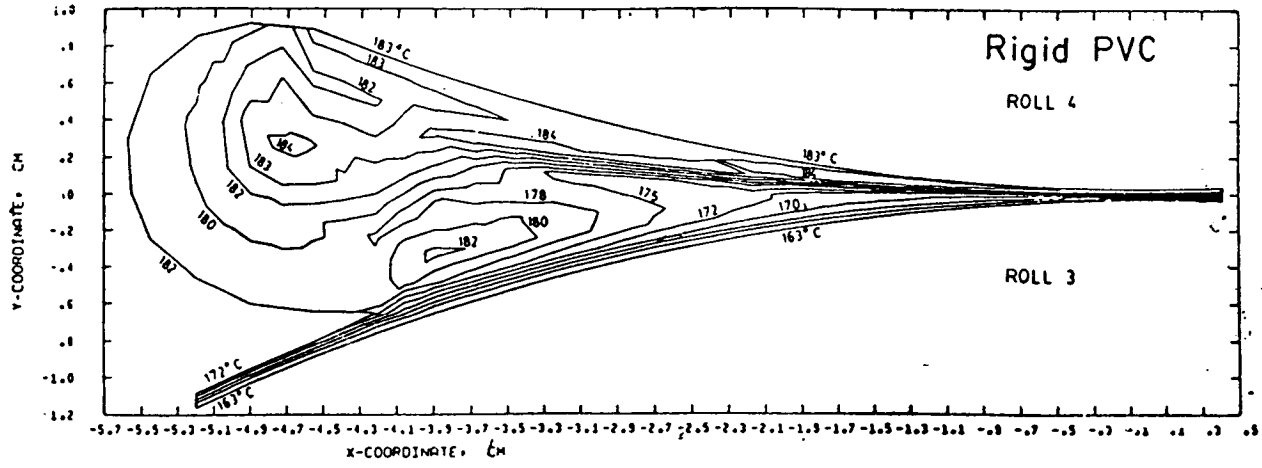

Fig. 14 Isotherms (same conditions as Fig. 13).

where ω_{ij} is the vorticity tensor given by

$$\omega_{ij} = (\partial v_i/\partial x_j - \partial v_j/\partial x_i) \tag{77}$$

The iterative scheme failed to converge for values of Deborah number larger than about 1.0. These numerical instabilities are encountered in all numerical calculations of viscoelastic flow (see for example Mitsoulis et al[61] and Crochet and Walters[66]). For Deborah number up to 1.0 the pressure distribution results were only slightly different from inelastic calculations and no definite trends could be detected.

The effect of normal stresses on pressure distribution can be approximately assessed (see also Tadmor and Gogos[3] and Middleman[47]) by starting from the momentum equation

$$0 = -\frac{\partial p}{\partial x} + \frac{\partial \tau_{xx}}{\partial x} + \frac{\partial \tau_{yx}}{\partial y} \tag{78}$$

Adding and subtracting $\partial \tau_{yy}/\partial x$ and then rearranging we get

$$\frac{\partial (\tau_{xx} - \tau_{yy})}{\partial x} + \frac{\partial \tau_{yx}}{\partial y} = \frac{\partial}{\partial y}(p - \tau_{yy}) \tag{79}$$

The first term is of the order of magnitude $[\tau_{xx} - \tau_{yy}]/[R]$ and the second term of the order $[\tau_{xy}]/[H_0]$ and their ratio is of the order

$$\left[\frac{\tau_{xx} - \tau_{yy}}{\tau_{yx}}\right]\left[\frac{H_0}{R}\right] \tag{80}$$

Since R would typically be $10^2 - 10^3$ times larger than H_0 and the stress ratio $(\tau_{xx} - \tau_{yy})/\tau_{yx}$ probably no larger than 10 before the onset of flow instability[60], we conclude that the normal stresses do not contribute much to the total pressure. It is possible however, that the normal stresses are responsible for flow pattern rearrangements in the melt bank. This topic is currently under investigation by the authors of the present review.

V. THREE-DIMENSIONAL FLOW

It is well known that the thermoplastic material spreads laterally as it enters the calender gap. This is due to the drag-induced pressure buildup which produces flow both in machine and cross-machine (axial) directions. This was clearly shown by Unkrüer[40] and apparently the combination of these forward and lateral motions (see Fig. 3) is responsible for the complex flow patterns observed. The complete three-dimensional analysis is in principle possible with the finite element method. It would, however, require a very large computer memory and large computer times because the boundary is not a priori known but must be determined iteratively. Such an analysis is quite impractical at the present time. It seems possible, however, to combine the two-dimensional model with a simplified (lubrication type) model in the axial direction. Such a model might explain, in

part at least, the discrepancies between the measured and predicted pressure distributions of Fig. 9. In fact a simple analysis indicates that the maximum pressure in the axial direction should have a parabolic distribution (maximum at the center and zero at the boundary) and this seems to be in qualitative agreement with Unkrüer's pressure profile measurements at different axial positions that were shown in Fig. 3 It is also interesting to note that for the data of Fig. 9 the sheet enters 22.5 cm wide and exists 37 cm wide. Since the pressure transducer was located on one cylinder 8 cm from the center we would expect a pressure approximately 20% lower than the maximum pressure, a result that is rather close to the measured value. Also, roll deflections (therefore larger gap) might have contributed to a reduction of measured pressure.

VI. CALENDERED SHEET AND FILM DEFECTS

There has been very little information on the origin and the characteristics of defects in calendered sheets. The discussion that follows is based entirely on Agassant's[28] comprehensive study on PVC. The calendered PVC defects can be classified into the following categories:

(a) **Dimensional Non-uniformities.** These are thickness variations in the machine or cross-machine direction due to the tendency of the rolls to bend under large separating forces. Compensations for roll deflections are provided by using crowned rolls having a larger diameter in the middle than at the ends, roll bending or roll skewing (see Meinecke[59]).

(b) **Structural Anomalies.** PVC exhibits certain particulate and crystalline structure changes under the influence of elevated temperature and stress which may lead to formation of defects in calendered sheets or films.

(c) **Mattness.** This is a micro-irregularity or loss of surface gloss that appears only on the surface that is not in contact with the roll after the sheet leaves the calender gap. This defect is apparently related to the phenomena of mattness, sharkskin and melt fracture in extrusion through capillary and slit dies[58,60]. Agassant[28] found that the onset of this defect occurs at a constant maximum wall shear stress value of about 5×10^5 Pa, which is about twice the critical stress for slit extrusion[60] of polystyrene.

(d) **V-shapes.** These are surface thickness irregularities (up to 3μ) in the form of more or less regular partially open V's with their vertices at the center of the sheet. According to Agassant[28] these V-shapes are

due to undulating motions in the melt bank that propagate from the centre to the edges.

(e) **Air Bubbles.** Bubbles of air are captured in the recirculating melt bank, pass through the calender gap and become elongated air enclosures in the sheet produced. High pressures that develop in the gap sometimes prevent these bubbles from passing through.

VII. CONCLUDING REMARKS

Most mathematical models of calendering are based on the lubrication approximation in one direction for Newtonian and shear-thinning materials. Slip at the wall is apparently necessary for the description of molten PVC flow through a calender gap. These models give reasonable predictions of pressure distribution, torque and power consumption. Two-dimensional finite element calculations permit the determination of the free surface and the recirculating flow pattern in the melt bank. Three dimensional flow occurs as the melt moves both in the machine and cross-machine directions. There has not been any analysis thus far to account for three-dimensional flow. Viscoelasticity may not be important in the determination of pressure and separating forces but may play an important role in vortex pattern formation in the melt bank.

There have been very few experimental studies and most of them with limited knowledge of melt properties. There is clearly a need for more experimental measurements of pressures, separating forces, torques and power consumption with polymers that have been subjected to a thorough rheological characterization. Also, more research on the origin and appearance of sheet and film defects is needed.

Acknowledgement

Financial assistance from the Natural Sciences and Engineering Research Council of Canada is gratefully acknowledged.

REFERENCES

1. R.A. Elden and A.D. Swan, *Calendering of Plastics*, American Elsevier, NewYork (1968).
2. D.I. Marshall, Chapter 6 in *Processing of Thermoplastic Materials*, E.C. Bernhardt, ed., Van Nostrand Reinhold, New York (1959), pp. 380-404.
3. Z. Tadmor and C.G. Gogos, *Principles of Polymer Processing*, Wiley, New York (1979).
4. G. Ardichvili, Kautschuk, **14**, 23 (1938).
5. D.D. Eley, J. Polym. Sci., **1**, 529 (1946).
6. D.D. Eley, J. Polym. Sci., **1**, 535 (1946).
7. M. Finston, J. Appl. Mech., **18**, 12 (1951).
8. R.E. Gaskell, J. Appl. Mech., **17**, 334 (1950).
9. P.R. Paslay, J. Appl. Mech, **24**, 602 (1957).
10. J.M. McKelvey, *Polymer Processing*, Wiley, New York (1962).
11. I. Brazinsky, H.F. Cosway, C.F. Valle, Jr., R. Jones, R. Clark and V. Story, J. Appl. Polym. Sci., **14**, 2771 (1970).
12. W.W. Alston and K.N. Astill, J. Appl. Polym. Sci., **17**, 3157 (1973).
13. G. Ehrmann and J. Vlachopoulos, *Rheol. Acta*. **14**, 761 (1975).
14. R. Ehrlich and J.C. Slattery, Ind. Eng. Chem. Fundamentals, **7**, No. 2, 239 (1968).
15. R. Takserman-Krozer, G. Schnenkel and G. Ehrmann, *Rheol. Acta*. **14**, 1066 (1975).
16. M. Renert, Materiale Plastice, **3** No. 3, 132 (1966).
17. E.D. Reher and L. Grader, Plast. Kautsch., **18**, 597 (1971).
18. R.V. Torner, *Grundprozesse der Verarbeitung von Polymeren*, VEB Deutscher Verlag für Grundstoffindustrie, Leipzig, G.D.R. (1974).
19. N. Tokita and J.L. White, J. Appl. Polym. Sci., **10**, 1011 (1966).
20. J.S. Chong, J. Appl. Polym. Sc., **12**, 191 (1968).
21. J.L. White, Rubber Chem. Technol., **42**, 257 (1969).
22. C. Kiparissides and J. Vlachopoulos, Polym. Eng. Sci., **16**, 712 (1976).
23. N.G. Bekin, V.V. Litvinov and V. Yu. Petrushanskii, Inter. Polym. Sci. Tech., 3. T/55 (1976).
24. C. Kiparissides and J. Vlachopoulos, Polym, Eng. Sci., **18**, 210 (1978).
25. F. Dobbels and J. Mewis, AIChEJ., **23**, 224 (1977).
26. J.F. Agassant and P. Avenas, J. Macromol Sci. Phys., **14**. 345 (1977).
27. J.L. Bourgeois and J.F. Agassant, J. Macromol. Sci. Phys., **14**, 367 (1977).

28. J.F. Agassant, *Le Calandrage des Matieres Thermoplastiques*, Doctoral Thesis, Univ. Pierre et Marie Curie, Paris 6 (1980).
29. J.G. Dimitrijew and E.A. Sporjagin, Plast. Kautsch, **24**, 484 (1977).
30. A.M. Woskressenski, W.N, Krassowski, L.K. Sewastjanow, C. Kohlert and E.O. Reher. Plast. Kautsch, **26**, 92 (1979).
31. R. Seeger, R Schnabel and E.O. Reher, Plast. Kautsch, **29**, 406 (1982).
32. J. Vlachopoulos and A.N. Hrymak, Polym. Eng. Sci., 20, 725 (1980).
33. T.S. Chung, J. Appl. Polym. Sci., **25**, 967 (1980).
34. T.S. Chung, J. Appl. Polym. Sci., 28, 2119 (1983).
35. S. Suto, K. Yamaguchi and T. Fujimura, Nih. Reo. Gakk. (J. Soc. Rheol. Japan), **8**, 103 (1980).
36. S. Suto and T. Fujimura, Kobunsh Ronb, 37, 627 (1980).
37. S. Suto, S. Suginuma and T. Fujimura, Kobunsh, Ronb, **40**, 17 (1983).
38. J.W. Lee. J.S. Yu and K.J. Lee, Proc 3rd PACHEC'83, Vol. 1, 69, Seoul, Korea (1983).
39. J.T. Bergen and G.W. Scott, J. Appl. Mech., 18 101 (1951).
40. W. Unkrüer, *Beitrag Zur Ermittlung des Druckverlaufes und der Fliessvorgänge im Walzspalt bei der Kalanderverarbeitung von PVC Hart zu Folien*, Doctoral Thesis, IKV, Techn. Hochsohule, Aachen, FRG (1970).
41. P. Prentice, Polymer, 22, 250 (1981).
42. G. Hatzmann, M. Herner and G. Müller, Ang. Markrom. Chem., 47, 257 (1975).
43. H. Kopsch, Ang Markrom. Chem., 47, 269 (1975).
44. J.C. Chauffoureaux, Solvay & Cie S.A., Brussels, Private Communication to J. Vlachopoulos (1980).
45. W.E. Langlois, *Slow Viscous Flow*, MacMillan, New York (1964).
46. J.R.A. Pearson, *Mechanical Principles of Polymer Melt Processing*, Pergamon Press, New York (1966).
47. S. Middleman, *Fundamentals of Polymer Processing*, Mc Graw-Hill, New York (1977).
48. J.C. Chauffoureaux, C. Dehennau and J. Van Rijckervorsel, J. Rheol., 21, 1 (1979).
49. C.F. Gerald, Applied Numerical Analysis, Addison-Wesley, Reading, MA (1978).
50. V. Yu. Petrusanskii and A.I. Sachaev, Ucenye Sapiski Jaroslavskogo Technologiceskogo Instituta, t. 23 (1971).
51. E. Mitsoulis, J. Vlachopoulos and F.A. Mirza, to appear in Polym. Proc. Eng.
52. E. Mitsoulis, J. Vlachopoulos and F.A. Mirza, "Finite Element Analysis of Calendering", Paper presented at IAMM Conference, Zurich Switzerland (August 1983).
53. E. Mitsoulis, J. Vlachopoulos and F.A. Mirza, "Calendering Analysis without the Lubrication Approximation", paper submitted for publication."
54. E. Mitsoulis, *Finite Element Analysis of Two-Dimensional Polymer Melt Flows*, Ph.D. Thesis, Dept. of Chemical Engineering, McMaster University, Hamilton, Ontario, Canada (1984).

55. E Mitsoulis, J. Vlachopoulos and F.A. Mirza, *MAVCIP-A Finite Element Program for Creeping Viscoelastic Flows*, Internal Report, Faculty of Engineering, McMaster University, Hamilton, Ontario, Canada (1983).
56. M.J. Crochet and K. Walters, Ann. Rev. Fluid Mech., 15, 241 ($16$83).
57. R.B. Bird, R.C. Armstrong and O. Hassager, *Dynamics of Polymeric Liquids*, Vol. I, Wiley (1977).
58. C.J.S. Petrie and M.M. Denn, AIChEJ. 22, 209 (1976).
59. E. Meinecke, *Calendering*, in Encyclopedia of Polymer Science and Technology, Vol. 2, Wiley, New York (1965), pp. 802–819.
60. J. Vlachopoulos and T.W. Chang, J. Appl. Pol. Sci., 21, 1177 (1977).